
A Simplified Method for Quantification of Myocardial Blood Flow Using Nitrogen-13-Ammonia and Dynamic PET

Yong Choi, Sung-Cheng Huang, Randall A. Hawkins, William G. Kuhle, Magnus Dahlbom, Carl K. Hoh, Johannes Czernin, Michael E. Phelps and Heinrich R. Schelbert

Division of Nuclear Medicine and Biophysics, Department of Radiological Sciences, Laboratory of Nuclear Medicine (DOE), Laboratory of Biomedical and Environmental Sciences and The Crump Institute for Biological Imaging, UCLA School of Medicine, Los Angeles, California*

The utility of Patlak graphical analysis was investigated for quantification of regional myocardial blood flow (MBF) and for generating parametric images of MBF with ^{13}N -ammonia and dynamic PET imaging in dogs and humans. MBF was estimated by a two-compartment model fit of the initial 2 min of the kinetic data and by Patlak graphical analysis of the initial 2, 3, or 4 min of data. In 11 dog studies, MBF by compartmental model fitting linearly correlated with MBF by microspheres (correlation coefficient (r) = 0.99, slope = 0.92) and by Patlak graphical analysis (r = 0.99, slope = 0.90). In 10 normal human studies, MBF obtained by the Patlak graphical analysis agreed well with MBF obtained by the compartmental model fitting (r = 0.96, slope = 1.04). Good agreement of the MBF estimates was also observed in 10 coronary artery disease patient studies (r = 0.96). Patlak graphical analysis permitted generation of parametric images of MBF. The parametric images of MBF, in units of ml/min/g, are of good image quality and have relatively low noise levels. We conclude that regional MBF can be noninvasively and conveniently measured with dynamic ^{13}N -ammonia PET using either a two-compartment model or Patlak graphical analysis. MBF parametric images generated with the Patlak graphical analysis both map the distribution and quantitate the magnitude of myocardial perfusion abnormalities.

J Nucl Med 1993; 34:488-497

Dynamic imaging with ^{13}N -ammonia and positron emission tomography (PET) permits the noninvasive quantification of regional myocardial blood flow (MBF). This noninvasive method has been validated in animals (1-6) and successfully applied to normal humans and patients with coronary artery disease (7-11).

Received Jul. 17, 1992; revision accepted Nov. 17, 1992.

For correspondence or reprints contact: Yong Choi, PhD, Division of Nuclear Medicine and Biophysics, Department of Radiological Sciences, UCLA School of Medicine, 10833 Le Conte Ave., Los Angeles, CA 90024-1721.

*Operated for the U.S. Department of Energy by the University of California under contract #DE-FC03-87ER60615.

Tracer kinetic models, either a two-compartment model (2,3) or a first-pass extraction method (6), for quantification of MBF utilizing ^{13}N -ammonia and PET produce estimates of MBF that are in good agreement with microsphere measurement in animals when corrected for the inverse relationship between the tracer first-pass extraction fraction and blood flow. Similarly, estimates of pharmacologically induced increase in myocardial blood flow with this approach in humans agree closely with those obtained with intracoronary Doppler flow velocity probes (9,12,13) and with those obtained with ^{15}O -water and PET under similar conditions (7-11,14-16).

This study was designed to test the hypothesis that the properties of ^{13}N -ammonia, which is avidly extracted and retained in myocardium, satisfy assumptions for Patlak graphical analysis. If this hypothesis proved to be correct, then regional MBF could be estimated via graphical analysis which would also permit generation of parametric images of MBF. Parametric (pixel-by-pixel) images of MBF provide quantitative information as well as a direct pictorial distribution of regional MBF in quantitative terms, analogous to parametric images of myocardial glucose utilization rates generated with dynamic PET-FDG imaging (17). The Patlak graphical analysis is computationally more efficient than the compartmental model approach and requires only linear regression rather than nonlinear regression. As compared to the first-pass extraction method, the approach fully utilizes the dynamic information of myocardial ^{13}N -ammonia uptake, while the first-pass extraction method uses one single static myocardial ^{13}N -ammonia uptake image.

MATERIALS AND METHODS

Animal Studies

A total of 11 studies, including 3 at baseline, 6 during dipyrindamole induced hyperemia, and 2 coronary occlusion studies in 4 mongrel dogs weighing 25 to 32.5 kg were included. Animal instrumentation and experimental procedures for these dog studies have been described in detail by Kuhle et al. (3). Four

arterial blood samples of 1 ml each were drawn at 40, 80, 120, and 180 sec after tracer injection for each study in order to determine the time-dependent distribution of ^{13}N -ammonia and its metabolites in whole blood (18,19).

Regional MBF for each study was measured independently with radioactive carbonized polystyrene microspheres (DuPont, North Billerica, MA). Simultaneously with the intravenous injection of ^{13}N -ammonia, approximately two million microspheres labeled with scandium-46, niobium-95, tin-113, or ruthenium-103 were injected over 15 sec into the left atrium. Arterial blood was withdrawn at a constant rate of 7.2 ml/min for 2 min and was later counted in a well counter for microsphere activity. After completion of the studies, the heart was removed, washed and cut into 1-cm thick left ventricular short-axis cross sections. After each section had been photographed, it was subdivided further into small 0.5 to 1 g sections, each of which was counted in a well counter for its microsphere activity concentration. Regional myocardial blood flow by microspheres (MBF_{MS}) was calculated by:

$$\text{MBF}_{\text{MS}} (\text{ml}/\text{min}/\text{g}) = C_t F_a / C_b, \quad \text{Eq. 1}$$

where F_a is the withdrawal rate of the arterial blood (ml/min), C_t is the microsphere activity concentration in a given myocardial region (cpm/g) and C_b is the total microsphere activity in the arterial blood sample (cpm) (20).

Human Studies

Two male and three female volunteers, ages 27 to 80 years (average 61 ± 21 yr) without evidence of cardiac disease and five patients with arteriographically documented coronary artery disease were studied. The study protocol was approved by the UCLA Human Subject Protection Committee and each participant gave informed consent in writing. The subjects were chosen to reflect a wide range of MBF in order to test the quantification methods in both normal and abnormal myocardium. Studies in each subject had been obtained at baseline and again, after dipyridamole induced myocardial hyperemia.

For the hyperemic study, dipyridamole (0.56 mg/kg) was infused for 4 min. Nitrogen-13-ammonia was injected at 4 min after the end of the dipyridamole infusion and when heart rate and blood pressure were stable.

Image Acquisition and Reconstruction

All dog and human studies were performed on a Siemens/CTI 931/08-12 tomograph. This device produces 15 simultaneous imaging planes encompassing a 108-mm axial field of view. A 2-min transmission scan with a $^{68}\text{Ge}/^{68}\text{Ga}$ external ring source was used to assist in centering the heart within the 15-plane axial field of view. A 20-min transmission scan was then acquired for subsequent photon attenuation correction.

Dogs and humans were injected intravenously over a 30-sec period, with about 20 mCi and 15 mCi, respectively, of ^{13}N -ammonia diluted in 10 ml saline solution. This intravenous line was then flushed with an additional bolus of 10 ml saline over a 30-sec interval.

Image acquisition was initiated simultaneously with ^{13}N -ammonia injection and consisted of a sequence of twelve 10-sec and six 20-sec frames in the dog studies and an image sequence of twelve 10-sec, two 30-sec, three 60-sec and one 900-sec frames in the human studies. Four gated frames, equally gated based on the electrocardiographic lead II signal, were acquired

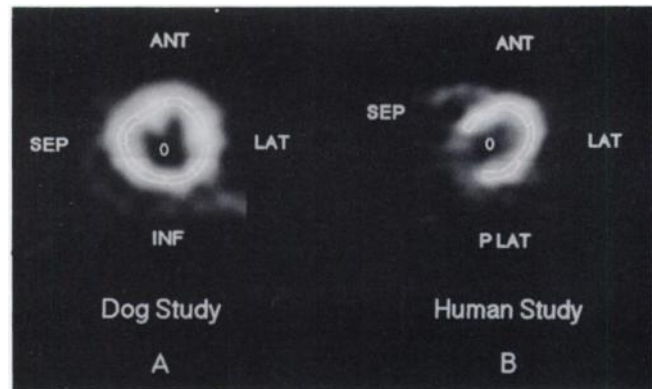


FIGURE 1. (A) Myocardial short-axis image obtained from a baseline dog study illustrates ROI definitions for canine studies. Anatomic locations of septum (SEP), anterior wall (ANT), lateral wall (LAT), and inferior wall (INF) are as indicated. (B) A transaxial image obtained from a dipyridamole-induced hyperemic study illustrates ROI definitions for normal human studies. Anatomic locations of septum (SEP), anterior wall (ANT), lateral wall (LAT) and posterolateral wall (PLAT) are as indicated. Small elliptical ROIs assigned to the left ventricular blood pool to derive arterial input functions are also illustrated in A and B.

immediately after the dynamic sequence for 20 min in dog studies. Repeat ^{13}N -ammonia studies were performed at 50–60-min intervals to allow for physical decay of ^{13}N activity from the prior study.

The serially acquired 15-plane transaxial images were reconstructed employing a Shepp-Logan filter with a cut-off frequency of 0.96 cycles/cm, yielding a spatial resolution of about 10 mm FWHM in plane. The scanner's axial resolution was approximately 7 mm FWHM.

Image Analysis and Recovery Coefficient Correction

In the dogs, the 15 contiguous transaxial images acquired in diastole as well as those acquired serially after tracer administration were reoriented into left ventricular short-axis slices as described previously (21). By using photographs of the postmortem myocardial cross sections as guides, three mid-ventricular planes of short-axis images were generated to match the three corresponding postmortem myocardial cross sections for each animal.

Eight sectorial myocardium time-activity curves were generated using ungated dynamic images from eight equally divided (45° for each sector) sectorial region of interests (ROIs) (Fig. 1A) defined by the two contours separated radially by three pixels (1.17 mm/pixel) and centered at the peak of myocardial circumferential activity. The myocardial contours were automatically drawn on each dynamic image frame, if the myocardial uptake was sufficiently high for defining myocardial edges. If myocardial uptake was not high enough in early frames, the myocardial contours and sectorial ROIs drawn on the later image frame were used. Usually, adequate definition of myocardial contours required an uptake period of 60 sec after injection. This auto-contouring was performed to minimize artifacts due to cardiac and respiratory motion or subject movement. Additional sets of myocardial tissue time-activity curves were generated by drawing contours and sectors on images obtained 2 min after injection and copying these sectorial ROIs to early or later dynamic

image frames to examine the motion effects on calculated myocardial blood flows.

Sectorial recovery coefficients for a given image spatial resolution, myocardial thickness and ROI thickness, in each imaging plane were based on the estimated myocardial activity thickness obtained by profile analysis of the activity across the myocardial wall on the diastolic gated images (22,23).

For the normal human studies, time-activity curves for four sectors (60° to 70° arcs assigned to the interventricular septum, the anterior, the lateral and the posterolateral wall) in one mid-ventricular transaxial plane were generated. Myocardial tissue time-activity curves for hypoperfused segments (17 segments) and normal segments (22 segments) in patients with coronary artery disease were generated by defining the sectors interactively. Three-pixel (1.56 mm/pixel) wide sectorial ROIs (Fig. 1B) were drawn on images obtained about 3 min after tracer injection. Sectorial myocardium time-activity curves were generated by copying these ROIs to the serially acquired transaxial dynamic image frames. The effects of partial volume were corrected with a constant recovery coefficient of 0.75 assuming a uniform myocardial activity thickness of 1 cm.

The time-activity curves of ¹³N activity concentrations in arterial blood, AB(t), were derived from a small elliptical ROI shown in Figure 1, with an area of about 50 mm², assigned to the left ventricular blood pool on the dynamic images (24,25). These curves were generated from two mid-ventricular imaging planes and were averaged to reduce noise. The fraction of ¹³N metabolites of the total ¹³N activity in whole blood was subtracted based on measurement in each dog study or, in human studies, based on previously reported results (19) to give the true arterial input function, C_a(t).

Calculation of MBF

Estimation of Regional MBF Using a Two-Compartment Model. The injected lipid soluble ¹³N-ammonia diffuses passively across the capillary and cell membranes into the cell and is converted to ¹³N-glutamine by the α-ketoglutarate-glutamate reactions and, more predominantly, by the glutamate-glutamine reaction (1). Because the intracellular glutamine pool is large and turns over very slowly, myocardial clearance half-times of the ¹³N label are longer than 100 min in canine myocardium and longer than 40 min in the isolated rabbit septum (1,26).

Based on the known uptake and retention mechanisms of ¹³N-ammonia in myocardium, a two-compartment mathematical model shown in Figure 2 was introduced to noninvasively quantify regional MBF (2,3,7,8). Q₁ (counts/pixel/min) represents ¹³N-ammonia activity in the freely diffusible compartment which includes both vascular and extravascular pools, and Q₂ (counts/pixel/min) represents the metabolically trapped ¹³N radioactivities. K₁ (ml/min/g) is the first order rate constant representing the conversion of freely diffusible ¹³N-ammonia into metabolically bound ¹³N-glutamine and k₂ (min⁻¹) is the clearance rate constant of ¹³N activities from the metabolite pool to the free ¹³N-ammonia pool. The term V (ml/g) represents the physical distribution volume of free ¹³N-ammonia in myocardium. C_a(t) is the arterial input function obtained from the left ventricular blood-pool ROI after correction for blood ¹³N-metabolites. SP_{bt} is the spillover fraction of activity from blood pool to myocardial tissue ROI.

At any time, t, after tracer injection, ¹³N radioactivity obtained from a myocardial tissue ROI, Q_i(t), is equal to the sum

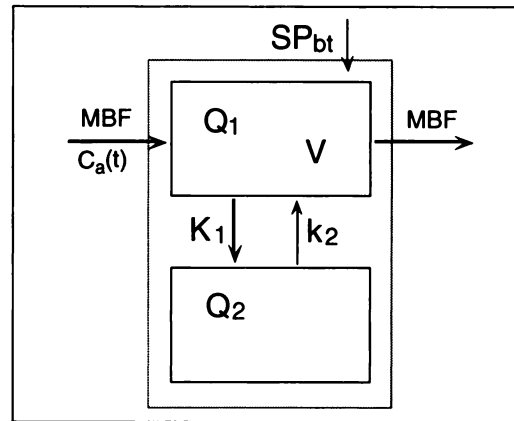


FIGURE 2. Two-compartment model represents the kinetics of ¹³N-ammonia in the myocardium. Q₁ and Q₂ represent ¹³N-ammonia activities (counts/pixel/min) in free and trapped spaces, respectively. V (ml/g) is the distribution volume of free ¹³N-ammonia in the myocardium. K₁ (ml/min/g) and k₂ (min⁻¹) are forward and reverse rate constants, respectively. SP_{bt} is the spillover fraction of activity from myocardial blood pool to myocardial tissue ROI.

of the activity of the free ¹³N-ammonia in the freely diffusible pool, Q₁(t), the activity of the ¹³N-metabolites in the bound pool, Q₂(t) and the spillover of activity from blood pool to myocardium ROI.

Therefore,

$$Q_i(t) = Q_1(t) + Q_2(t) + SP_{bt} \cdot AB(t), \quad \text{Eq. 2}$$

where AB(t) is ¹³N radioactivity in arterial blood. The rate of radioactivity change in the freely diffusible compartment and that in the trapped compartment in myocardium, dQ₁(t)/dt and dQ₂(t)/dt respectively, can be described by the following equations:

$$\frac{dQ_1(t)}{dt} = -\frac{K_1 + MBF}{V} Q_1(t) + k_2 Q_2(t) + MBF \cdot C_a(t) \quad \text{Eq. 3}$$

$$\frac{dQ_2(t)}{dt} = \frac{K_1}{V} Q_1(t) - k_2 Q_2(t), \quad \text{Eq. 4}$$

where MBF is myocardial blood flow in ml/min/g. MBF can be obtained by solving these differential equations describing the two-compartment model and by fitting to the myocardial tissue time-activity curves. The rate constant k₂ was assumed to be zero during the first 2 min after tracer injection because of the relatively long clearance half-times of trapped ¹³N activity and V was fixed at 0.8 ml/g as established previously (2). During the model fitting, the relationship between K₁ and MBF,

$$K_1 = MBF[1.65e^{(1.25/MBF)} - 1] \quad \text{Eq. 5}$$

which is derived by equating the extraction fraction (E_m) from the two-compartment model,

$$E_m = \frac{K_1}{K_1 + MBF} \quad \text{Eq. 6}$$

to the extraction fraction (E_d) determined previously (I) in a series of dog experiments

$$E_d = 1 - 0.607e^{(-1.25/MBF)} \quad \text{Eq. 7}$$

was used to reduce the number of variable parameters.

Estimation of Regional MBF and Generation of Parametric Images of MBF Using Patlak Graphical Analysis. Integration of Equations 3 and 4, assuming k_2 is negligible, results in:

$$Q_1(t) = -\frac{K_1 + MBF}{V} \int_0^t Q_1(t)dt + MBF \int_0^t C_a(t)dt \quad \text{Eq. 8}$$

$$Q_2(t) = \frac{K_1}{V} \int_0^t Q_1(t)dt. \quad \text{Eq. 9}$$

By substituting $Q_1(t)$ and $Q_2(t)$ in Equation 2, expressing the time integral of $Q_1(t)$ in terms of that of $C_a(t)$ (using Equation 8) and using the relationship that $Q_1(t) = MBF \cdot V(K_1 + MBF) C_a(t)$ at large t (when $dQ_1(t)/dt \rightarrow 0$), one can obtain the following Patlak equation:

$$\frac{Q_i(t)}{C_a(t)} = K \frac{\int_0^t C_a(\tau)d\tau}{C_a(t)} + \frac{MBF^2V}{(MBF + K_1)^2} + SP_{bt} \frac{AB(t)}{C_a(t)}, \quad \text{Eq. 10}$$

where K , the slope of the straight portion of the Patlak plot indicating delivery from arterial input to the precursor pool times the fraction trapped in the bound pool, is expressed as follows:

$$K = MBF \frac{K_1}{MBF + K_1}. \quad \text{Eq. 11}$$

By using Equations 6 and 7, Equation 11 can be expressed as:

$$K = MBF \cdot E_m = MBF \cdot E_d \quad \text{Eq. 12}$$

and

$$K = MBF [1 - 0.607e^{(1.25/MBF)}]. \quad \text{Eq. 13}$$

Thus, MBF can be measured, with the assumption that $k_2 = 0$, by estimating the slope, K , of the straight portion of the graph, $Q_i(t)/C_a(t)$ (vertical (y) axis) versus $\int_0^t C_a(\tau)d\tau/C_a(t)$ (horizontal (x) axis) and by using the relationship described in Equation 13. A linear regression equation was applied either to sectorial myocardial time-activity curves generated from sectorial ROIs on dynamic images to calculate regional MBF or to each image pixel of dynamic image frames to generate parametric images of MBF.

In the above discussion, the term $SP_{bt} \cdot AB(t)/C_a(t)$ in Equation 10 is assumed to be constant. In real cases when there are labeled metabolites, $AB(t) \neq C_a(t)$. Thus, $SP_{bt} \cdot AB(t)/C_a(t)$ varies as a function of time. However, for a short time after tracer injection (for example, 2 min), the concentration of labeled metabolites is small, and the time dependency of the term does not significantly affect either the slope or the intercept of the Patlak plot. Therefore, $AB(t)/C_a(t)$ is assumed to equal one for the time intervals used in analyzing the Patlak plot.

The intercept of the Patlak plot, $MBF^2V/(MBF + K_1)^2 + SP_{bt}$, can be simplified using Equation 5 to:

$$\frac{MBF^2V}{(MBF + K_1)^2} + SP_{bt} = 0.37Ve^{-(2.5/MBF)} + SP_{bt}. \quad \text{Eq. 14}$$

Note that the intercept of the Patlak plot is relatively small because of the high extraction fraction of ^{13}N -ammonia. The value for the intercept of the Patlak plot should be larger than SP_{bt} and should be smaller than $(0.22 \text{ ml/g} + SP_{bt})$ (when $V \approx 1.0 \text{ ml/g}$ and $MBF \approx 5 \text{ ml/min/g}$) for blood flows in the physiologic range. The average of SP_{bt} estimated from a two-compartment model fitting without recovery coefficient correction was 0.43 ± 0.11 (ranging from 0.72 to 0.2) for 40 myocardial sectors in 10 normal studies [if the partial volume effect was corrected using a recovery coefficient of 0.75, the average of SP_{bt} will be $0.57 (0.43/0.75)$].

The impact of constraining the intercept of the Patlak plot was also evaluated. The intercept of the Patlak plot was constrained within the physiologically acceptable range to examine if this constraint improves the correlation between the MBF estimated by the Patlak graphical analysis and the MBF estimated by microspheres or by the two-compartment model fitting. After estimating the slope and the intercept of the Patlak plot without any constraints, the intercept value was examined. If it was within the acceptable range discussed above, the slope of the Patlak plot was accepted. However, if it was smaller than the lower limit, it was fixed to the value of 0.43, which is the average value of SP_{bt} in normal humans. If it was larger than the upper limit, it was fixed to 0.65, which is the sum of 0.22 ml/g and the average value of SP_{bt} . Then the new slope of the Patlak plot was calculated using the following linear regression equation:

$$K = \left\{ \sum_{i=m}^n X_i Y_i - (\text{the new intercept}) \sum_{i=m}^n X_i \right\} / \sum_{i=m}^n X_i^2, \quad \text{Eq. 15}$$

where X_i and Y_i represent, respectively, the horizontal and vertical coordinates of each kinetic data point used in Equation 10, m is the first frame number and n is the last frame number of the dynamic image frames used for the slope determination, and (the new intercept) indicates either the lower limit or the upper limit value of the ordinate intercept of the Patlak plot. The spillover fraction, SP_{bt} , estimated in normal human studies was also used in dog studies.

We also examined the effect of the number of time points used in the Patlak analysis on the estimated slope K of the Patlak plot and the resultant MBF estimate, and on the noise level in the generated parametric images of MBF.

RESULTS

Dog Studies

Figure 3A shows an ^{13}N -metabolite corrected arterial input curve and one normal sectorial myocardial tissue time-activity curve obtained from a baseline dog study. It demonstrates the good statistical quality of the kinetic data and the model fit (from 0 to 120 sec) using nonlinear regression and the two-compartment model. The Patlak plot of normalized counts, $Q_i(t)/C_a(t)$, versus normalized time, $\int_0^t C_a(\tau)d\tau/C_a(t)$, for the same data set illustrates the

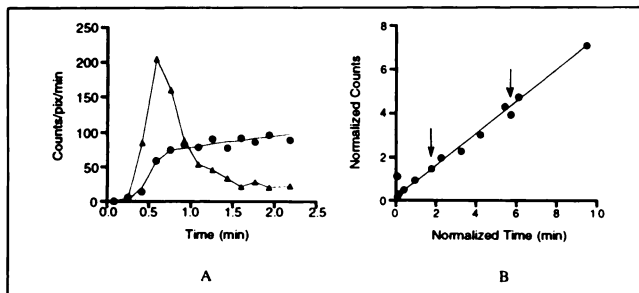


FIGURE 3. (A) Arterial input function (filled triangles) derived from ROI in the left ventricular blood pool and a myocardial tissue time-activity curve (filled circles) derived from a sectorial ROI in normal myocardium in a baseline canine study. The smooth line through the myocardium kinetic data is the two-compartment model fit to the data obtained from 0–2 min after injection. A line (linear interpolation) was also drawn through the input function data to illustrate the shape of the curve. (B) The Patlak plot of normalized time versus normalized counts for the same data set of A. Filled circles are data points, while the straight line is a linear fit to the data from 70–120 sec, marked by arrows, after tracer injection.

high quality (correlation coefficient = 0.99) of the linear fit (from 70 to 120 sec) (Fig. 3B).

Myocardial blood flow determined with the microsphere method ranged from 0.5 to 4.2 ml/min/g. As shown in Figure 4, MBF estimated by the two compartment model and nonlinear fitting routines correlates well with the microsphere measured blood flow values. Linear regression line demonstrated a strong relationship between both estimates (slope of 0.92, intercept of 0.06 ml/min/g and a correlation coefficient of 0.99).

Figure 5 depicts the correlation of regional MBF estimates for 264 segments (8 sector/plane \times 3 plane/study \times 11 studies) obtained by the two-compartment model fitting and by the Patlak graphical analysis in the dog experiments. The myocardial tissue data recorded from 0 to

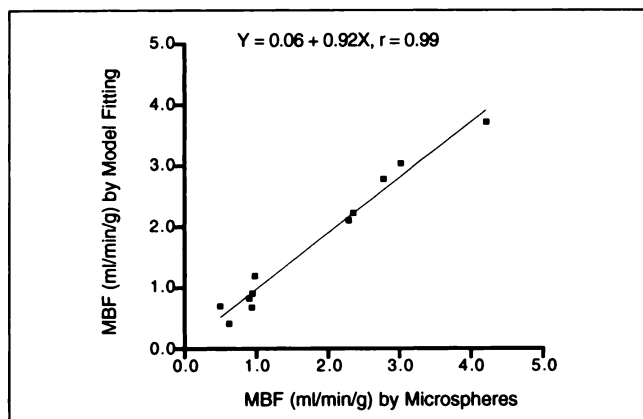


FIGURE 4. Comparison of MBF estimates by microspheres and by the two-compartment model fitting using 0–2 min kinetic data in 11 dog studies. Flow values are averages over the midventricular myocardium for each study. The straight line, $Y = 0.06 + 0.92X$, $r = 0.99$, is a linear regression fit to the data.

120 sec after injection were used in the model fitting and those recorded from 70 to 120 sec were used in the Patlak graphical analysis. Note the excellent correlation of regional MBF estimates over a wide range of MBF not only in baseline and hyperemic studies but also in hypoperfused regions. The correlation was further improved (Fig. 5B) by constraining the intercept of the Patlak plot as expressed in Equation 14 and described earlier.

Patlak graphical analysis can be used for generating parametric images of MBF by applying Equations 10 and 13 to image values in each pixel. The computation time for a 128×128 image is about 10 sec with a MicroVAX 3200. Figure 6 includes images of one myocardial short-axis cross section at 2 min after tracer injection at baseline and after dipyridamole-induced hyperemia in a dog and the corresponding parametric images of MBF. The myocardial kinetic data at 70–120 sec after tracer injection were used without constraining the intercept of the Patlak plot for generating these parametric images. An increase in MBF (from 0.8 ml/min/g in baseline study to 2.7 ml/min/g in the dipyridamole study measured by microspheres) is well visualized in the parametric images (from 0.8 ml/min/g to 2.6 ml/min/g). Also note the increased contrast of myocardium to background on the parametric images when compared to the count density images.

Figure 7 illustrates a comparison of the Patlak estimated MBF values obtained from myocardial tissue time-activity curves generated by drawing contours on each dynamic image frame of 70 to 120 sec after injection (autocontouring) versus the estimates obtained from curves generated by copying contours drawn on image frame of 120 sec to earlier dynamic image frames. The ordinate intercept of the Patlak plot was not constrained for both estimates. The method of copying ROIs did not account for cardiac and respiratory motion and tended to underestimate MBF estimates, although the magnitude of this underestimation was small. Despite several outlier points due to the inherent noise sensitivity of the linear Patlak fit and the relatively small sector size used (45° for each sector), a good correlation was observed ($r = 0.95$).

Human Studies

Although the qualities of human arterial input and myocardial tissue kinetic data are noisier than those of dog studies (Fig. 3) because of the lower injected dose per unit body weight in human studies, the two-compartment model still fitted the kinetic data well and was consistent with previous studies (7,8). The linear fit to the Patlak kinetic data for human studies also showed good quality.

A comparison of MBF estimates for 40 myocardial segments in 10 baseline and hyperemic normal human studies generated with the two-compartment model fitting and with the Patlak graphical analysis is shown in Figure 8. The MBF values estimated by model fitting using the kinetic data from 0 to 120 sec after tracer injection ranged

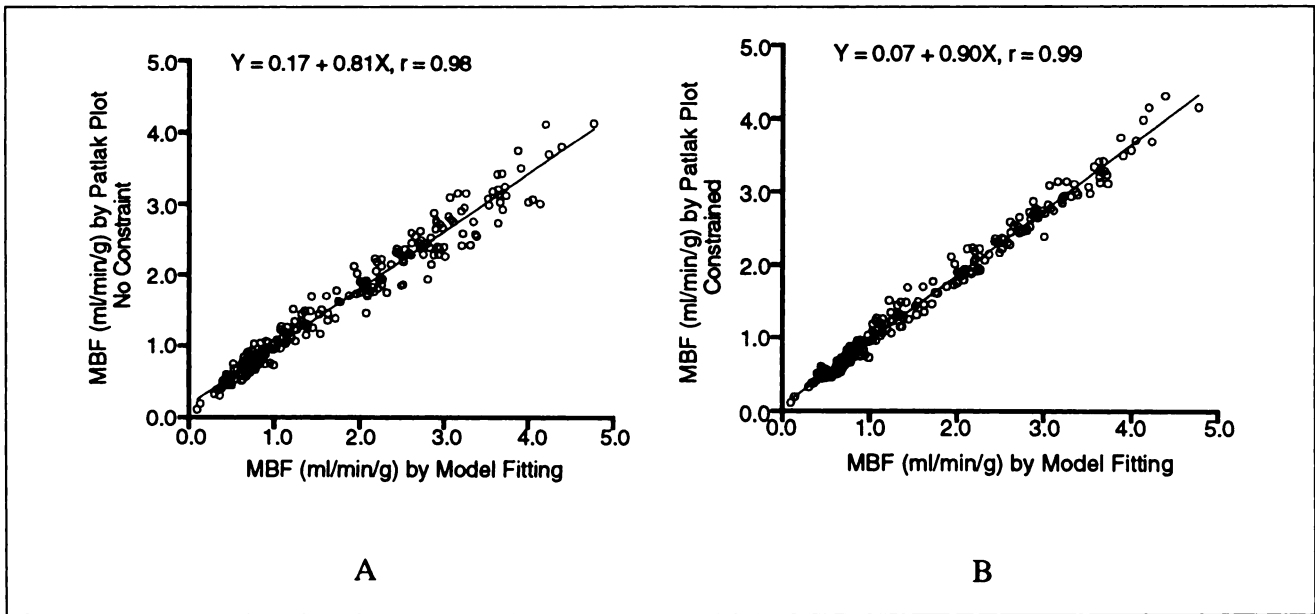


FIGURE 5. Comparison of regional MBF estimated by two-compartment model fitting and Patlak graphical analysis for 264 myocardial segments. Myocardial tissue data points obtained from 70 to 120 sec after injection were used for the graphical analysis. The MBF estimates obtained with Patlak graphical analysis in A were produced without any intercept constraint, while those in B were estimated with an intercept constraint. The regression lines and correlation coefficients were $Y = 0.17 + 0.18X$, $r = 0.98$ (A) and $Y = 0.07 + 0.90X$, $r = 0.99$ (B).

from 0.48 to 2.75 ml/min/g. The correlation of MBF estimates obtained with the two methods increased from 0.82 for data without an intercept constraint on the Patlak graphical analysis (Fig. 8A) to 0.96 for data with the constraint (Fig. 8B). Additionally, the high correlation was preserved as the number of data points used in the Patlak analysis was increased to include acquisition times of 165 sec (Fig. 8C) and up to 210 sec (Fig. 8D) although the slope of the linear regression line decreased from 1.04 to 0.83 and to 0.75, respectively.

Figure 9 includes a comparison of estimates of regional MBF by the compartment model and by Patlak graphical analysis in normal and hypoperfused segments in 10 coronary artery disease patient studies performed in baseline and in dipyridamole-induced hyperemic states. The intercept was constrained within the range derived from the normal volunteer studies for the results of the Patlak graphical analysis (70–120 sec). A good correlation between the two methods, $r = 0.96$, was evident in this group of hypoperfused and normal segments.

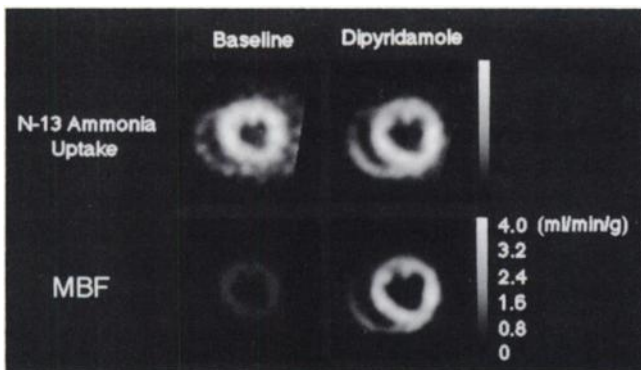


FIGURE 6. Short-axis slice of ^{13}N -ammonia count density images of a single plane obtained 2 min after tracer injection at baseline (upper left panel) and after dipyridamole (upper right panel) in a dog and the corresponding parametric images (lower panels). Parametric images of MBF are scaled to units of ml/min/g.

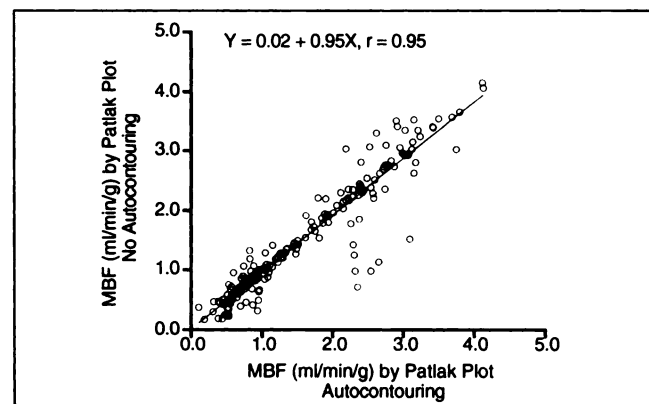


FIGURE 7. Comparison of MBF values generated by autocontouring (horizontal axis) and those generated by copying ROIs drawn on image frame of 120 sec to earlier dynamic image frames (vertical axis). The MBF values were estimated by Patlak graphical analysis using myocardial time-activity curves from 70 to 120 sec after tracer injection. The straight line ($Y = 0.02 + 0.95X$, $r = 0.95$) is the linear fit to the data.

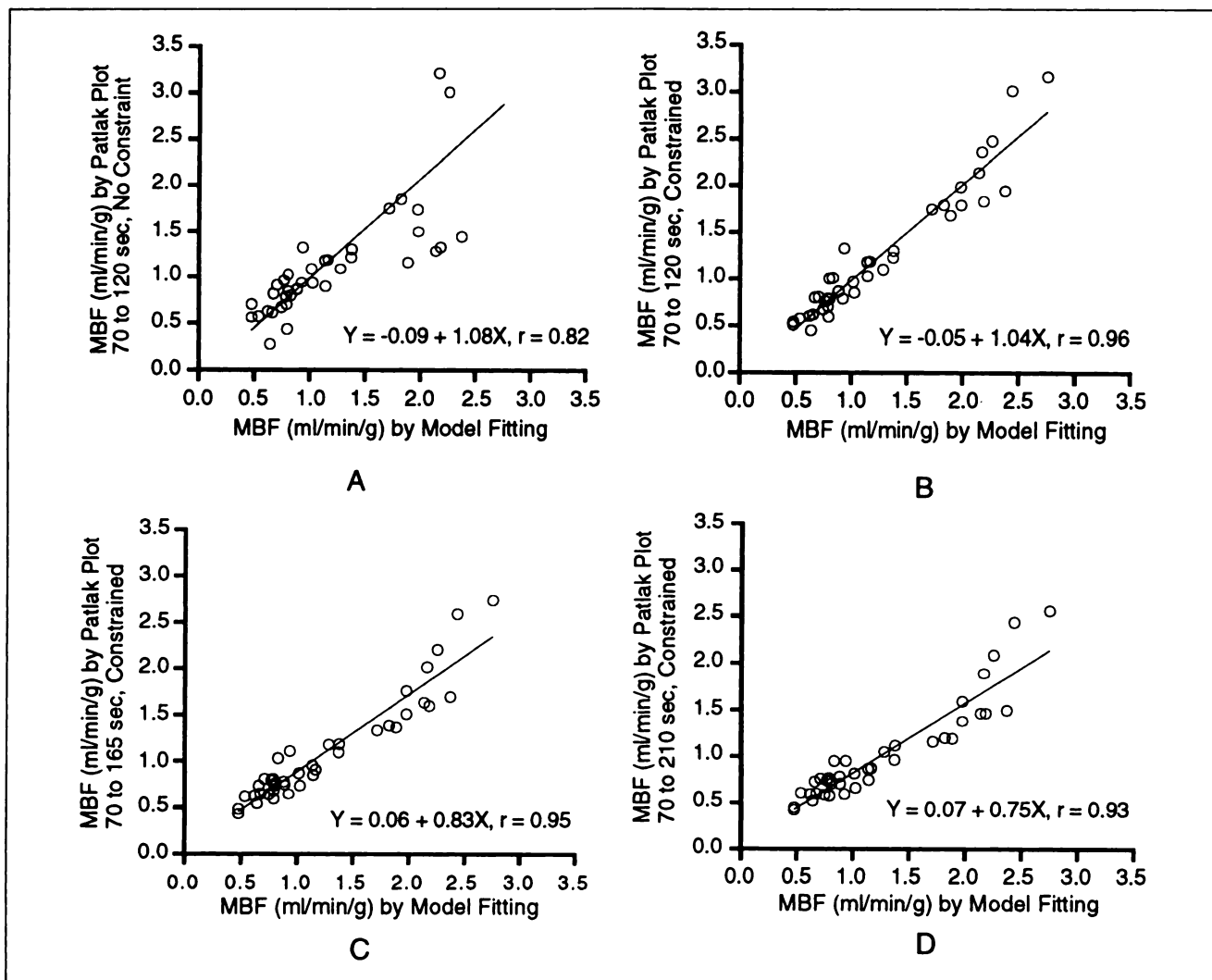


FIGURE 8. Comparisons of MBF estimates in normal human volunteers obtained with the two-compartment model using data 0 to 120 sec following tracer injection (horizontal axis) to those obtained with Patlak graphical analysis (vertical axis) without any constraint (A) and with a constraint on the intercept of the Patlak plot (B, C and D). Patlak analysis was performed using 70–120-sec myocardial kinetic data (A and B), 70–165-sec data (C) and 70–210-sec data (D). The linear regression lines and correlation coefficients for MBF estimates are $Y = -0.09 + 1.08X$, $r = 0.82$ (A), $Y = -0.05 + 1.04X$, $r = 0.96$ (B), $Y = 0.06 + 0.83X$, $r = 0.95$ (C) and $Y = 0.07 + 0.75X$, $r = 0.93$ (D).

A subset of dynamic images from a dipyridamole-induced hyperemic study in a normal subject is illustrated in the upper panels of Figure 10. The ^{13}N radioactivity bolus is observed first in the ventricular chambers, and the activity then progressively accumulates in the myocardium. The lower panels of Figure 10 include the parametric images of MBF generated by Patlak graphical analysis of the dynamic images in the upper panels. The parametric image generated using dynamic images of 70–120 sec after injection without any intercept constraint on the Patlak graphical analysis is noisy. Image quality is improved by constraining the intercept within the physiological range and by including the later time points, which reduce noise statistics, in the analysis.

DISCUSSION

This study indicates that the Patlak graphical analysis of kinetic ^{13}N -ammonia PET data is an efficient and accurate approach for quantifying regional myocardial blood flow. The MBF estimates obtained by two-compartment model fitting and by Patlak analysis correlated well with the values obtained by microsphere measurements in dog studies (Figs. 4, 5 and 6) and demonstrated a consistent increase after dipyridamole administration in human studies (Figs. 8 and 9). The excellent correlation of the MBF estimates obtained by the two-compartment model and by the model-independent Patlak graphical analysis (Figs. 5, 8 and 9) indicates that both approaches produce accurate estimates of regional MBF.

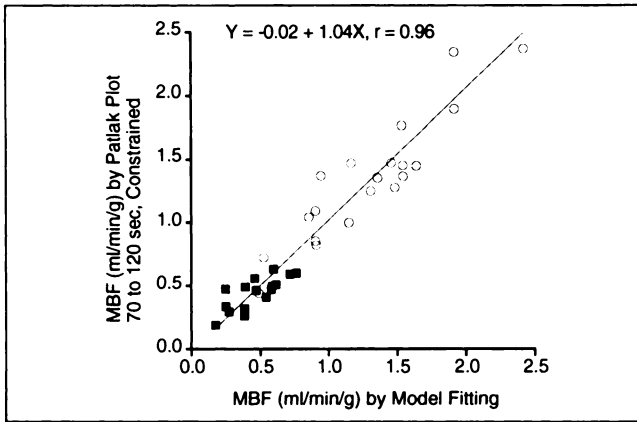


FIGURE 9. Comparison of the MBF estimates obtained with model fitting and those from Patlak graphical analysis for 17 hypoperfused (filled squares) and 22 normal (open circles) myocardial segments in five patients with coronary artery disease. The intercept of the Patlak plot was constrained and myocardial tissue data from 70 to 120 sec after injection were used in the Patlak graphical analysis. The linear regression line and correlation coefficient for MBF estimates with the two methods was $Y = -0.02 + 1.04X$, $r = 0.96$.

Intercept Constraint on the Patlak Plot. The correlation of MBF estimates obtained by the model fitting and by the Patlak graphical analysis improved considerably when the intercept of the Patlak plot was constrained within a theoretically and physiologically permissible range in animals and in humans. The constraint stabilizes

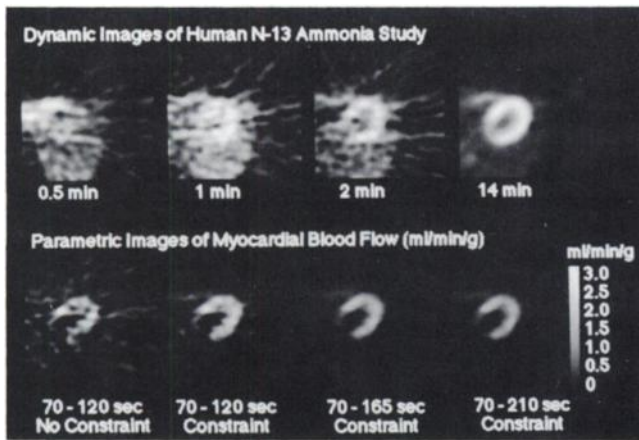


FIGURE 10. (Upper panels) Selected dynamic PET images of ^{13}N -ammonia after intravenous dipyridamole in a normal human volunteer. The times below each image denote the middle of the scan time of the image acquisition. The scan durations of the four images were (from left image) 10, 10, 10 and 900 sec. (Lower panels) Parametric images of MBF generated using the dynamic images in the upper panels and Patlak graphical analysis. The time points included in the Patlak graphical analysis were from data 70–120 sec (the first and the second images from left), 70–165 sec (the third image) and 70–210 sec (the fourth image) after injection. The intercept of the Patlak plot was not constrained for the first image, while the intercept was constrained for the other parametric images.

the linear fit of the Patlak plot for noisy kinetic data by limiting the intercept to a physiologically acceptable range, and by reducing the estimated variables from two to one. Limiting the intercept of the Patlak plot is required in statistically noisier human studies in order to obtain MBF estimates close to the model estimates and to obtain parametric images with acceptable noise levels.

Comparison of MBF Estimates Obtained by Model Fitting and by Patlak Graphical Analysis. The slope of the linear regression line of the MBF estimates obtained by two-compartment model fitting and by Patlak graphical analysis was 0.9 in dog studies (Fig. 5) and about 1.0 in human studies (Fig. 8B). The underestimation of the flow values estimated by the Patlak graphical analysis became apparent when 70–165 sec myocardium data were used in the human studies and became more obvious when data from 70 to 210 sec were used.

The underestimation of MBF values by Patlak graphical analysis in the animal and human studies may have resulted from inaccurate estimation of arterial input functions. Arterial input functions derived from the time-activity curves of the left ventricular blood pool can be contaminated by ^{13}N -metabolite activities in arterial blood and by the spillover of activity from the myocardium to blood pool. While the input functions of the two-compartment model can also be contaminated by these two sources, the Patlak graphical analysis employed 70–120, 70–165 or 70–210 sec of myocardium data (the first 60 sec of myocardium data were excluded), while model fitting employed data from 0 to 120 sec after injection. Therefore, Patlak graphical analysis is more affected by inaccuracies related to input functions because contamination of the input function either from ^{13}N -metabolites or from spillover from myocardial tissue to blood pool become more prominent at later scan times. These errors in arterial input functions were more obvious in dog studies than in human studies because of faster metabolism of ^{13}N -ammonia in blood and because of faster accumulation of ^{13}N activity in the relatively smaller canine heart (19). Therefore, the slight underestimation of MBF values by the Patlak graphical analysis employing 70–120 sec myocardial data was observed only in dog studies. The ^{13}N -metabolite fraction in whole blood in human studies was corrected based on the mean distribution of radioactivity in nine human whole blood studies reported by Rosenspire et al. (19). According to their results, the percentage of ^{13}N -ammonia in arterial blood is 94.0 ± 2.8 at 2 min after tracer injection, which indicates that ^{13}N -metabolite fraction seen early after tracer injection is small. The amount of error due to the variance of ^{13}N -metabolites between subjects will be negligible after the correction based on the reported value. Patlak graphical analysis could underestimate flow values if k_2 in the two-compartment ^{13}N -ammonia model is not zero (17,25,27,28). The underestimation of MBF by the Patlak graphical analysis therefore can also be explained

by a non-zero k_2 . However, the fraction of this underestimation due to a non-zero k_2 is small because of the long clearance half-time of metabolically bound ^{13}N activities from the myocardium.

The best time interval to use in Patlak graphical analysis depends on the noise level of the data. For regional myocardium, the MBF estimates obtained by Patlak graphical analysis using 70–120-sec data points are as accurate as those obtained by the two-compartment model in both dog and human studies. For parametric images, good quality images can be generated by Patlak graphical analysis using 70–120-sec data points in dog studies and 70–165-sec data points in human studies. The underestimation of MBF values should be corrected when 70–165-sec data points were used by adjusting the estimated flow values by a factor of 1/0.83 (Fig. 8C).

Advantages of Patlak Graphical Analysis. The MBF estimates by Patlak graphical analysis are expected to be more reliable than those from the first-pass extraction method (6) because Patlak graphical analysis utilizes more and/or earlier data points of ^{13}N -ammonia uptake kinetics in the myocardium. For instance, MBF estimates by Patlak graphical analysis using 70–120-sec myocardial data utilize myocardial ^{13}N -ammonia uptake kinetics measured at six different time points, while the first-pass extraction method uses a single frame image at a specific time, for example, 2, 3 or 10 min after tracer injection. The ^{13}N -ammonia kinetics in arterial blood and in the myocardium have been relatively well characterized within the first few minutes after ^{13}N -ammonia injection, but they become more complicated and difficult to characterize at later times. For example, the clearance of labeled metabolite from the myocardium and/or the uptake of labeled metabolites from plasma at later times could potentially affect the estimated MBF value of the first-pass extraction method. In addition, the spillover fraction of radioactivities from the left ventricular chamber to myocardium, SP_{bv} , can be taken into account in Patlak graphical analysis as the intercept of the Patlak plot, while the first-pass extraction method inherently assumes a zero spillover fraction and a zero intercept, which can overestimate blood flow especially in hypoperfused regions.

Graphical analysis is computationally much faster than compartment modeling approaches because it requires only linear regression rather than nonlinear regression and can be used for generating pixel-by-pixel parametric images of MBF. Our results indicate that MBF estimates obtained by Patlak graphical analysis are as reliable as those obtained by model fitting (Figs. 5, 8 and 9).

Parametric imaging approaches are usually vulnerable to movement artifacts. However, the parametric images of MBF generated by the method shown in this study are relatively insensitive to movement problem because the method requires only the first 2 or 3 min of data. Parametric images have the advantage of facilitating numeri-

cal evaluation of regional MBF and can compress numerous image frames of dynamic PET studies into a single parametric image.

Partial Volume Effect Correction in Human Studies. Partial volume effects were corrected in this study using a constant recovery coefficient in human studies because the primary purpose of the human studies was the validation of Patlak graphical analysis by comparing MBF estimates obtained by Patlak graphical analysis to those from the modeling approach. Strictly speaking, the recovery coefficient is not constant, especially in the regions containing papillary muscles and in the patients studies. However, errors due to the use of constant recovery coefficients will affect MBF estimates of both approaches and thus have minimal effects on the comparison results.

Applications of Patlak Graphical Analysis. Nitrogen-13-ammonia kinetics in some other organs, such as kidneys and liver (29,30), have been reported to be similar to those in the myocardium, although first-pass extraction fractions vary in different organs. Patlak graphical analysis can be applicable for estimating tracer extraction and thus blood flow in these organs with ^{13}N -ammonia and dynamic PET similar to what is shown in this study.

CONCLUSIONS

Regional MBF can be quantified with dynamic ^{13}N -ammonia PET and the two-compartment model. Regional MBF estimates obtained by Patlak graphical analysis are as reliable as those obtained by two-compartment model fitting. The computationally efficient Patlak graphical analysis facilitates quantification of regional MBF. Low noise parametric images and also parametric polar maps of MBF can be generated. The parametric imaging approach has the advantage of compressing large amount of data from dynamic PET studies into a single parametric image and facilitates evaluation of absolute quantities of flow abnormalities and their geographic extent and distribution.

ACKNOWLEDGMENTS

The authors thank Ron Sumida, Larry Pang, Francine Aguilar, Sammy Chan, MD, N. Satyamurthy, PhD and Eileen Rosenfeld for their help in performing this project. This work was supported in part by the Director of the Office of Energy Research, Office of Health and Environmental Research, Washington, DC and by research grants HL 29845 and HL 33177 from the National Institutes of Health, Bethesda, MD.

REFERENCES

1. Schelbert HR, Phelps ME, Huang SC, et al. N-13 ammonia as an indicator of myocardial blood flow. *Circulation* 1981;6:1259–1272.
2. Smith GT, Huang SC, Nienaber CA, Krivokapich J, Schwaiger M, Schelbert HR. Noninvasive quantification of regional myocardial blood flow with N-13 ammonia and dynamic PET [Abstract]. *J Nucl Med* 1988;29:950.

3. Kuhle W, Porenta G, Buxton D, et al. Quantification of regional myocardial blood flow using N-13 ammonia and reoriented dynamic positron emission tomographic imaging. *Circulation* 1992;86:1004-1017.
4. Shah A, Schelbert HR, Schwaiger M, et al. Measurement of regional myocardial blood flow with N-13 ammonia and positron-emission tomography in intact dogs. *J Am Coll Cardiol* 1985;5:92-100.
5. Nienaber CA, Ratib O, Gambhir SS, et al. A quantitative index of regional blood flow in canine myocardium derived noninvasively with N-13 ammonia and dynamic positron emission tomography. *J Am Coll Cardiol* 1991;17:260-269.
6. Bellina CR, Parodi O, Camici P, et al. Simultaneous in vitro and in vivo validation of nitrogen-13-ammonia for the assessment of regional myocardial blood flow. *J Nucl Med* 1990;31:1335-1343.
7. Krivokapich J, Smith GT, Huang SC, et al. N-13 ammonia myocardial imaging at rest and with exercise in normal volunteers: quantification of absolute myocardial perfusion with dynamic positron emission tomography. *Circulation* 1989;80:1328-1337.
8. Krivokapich J, Stevenson LW, Kobashigawa J, Huang SC, Schelbert HR. Quantification of absolute myocardial perfusion at rest and during exercise with positron emission tomography after human cardiac transplantation. *J Am Coll Cardiol* 1991;18:512-517.
9. Hutchins GD, Schwaiger M, Rosenspire KC, et al. Noninvasive quantification of regional blood flow in the human heart using N-13 ammonia and dynamic positron emission tomographic imaging. *J Am Coll Cardiol* 1990;15:1032-1042.
10. Hara T, Michihata T, Yokoi F, et al. Quantitative measurement of regional myocardial blood flow in patients with coronary artery disease by intravenous injection of ¹³N-ammonia in positron emission tomography. *Eur J Nucl Med* 1990;16:231-235.
11. Yoshida K, Endo M, Himi T, et al. Measurement of regional myocardial blood flow in hypertrophic cardiomyopathy: application of the first-pass flow model using [¹³N]ammonia and PET. *Am J Physiol Imaging* 1989;4:97-104.
12. Wilson RF, Laughlin DE, Ackell PH, et al. Transluminal, subselective measurement of coronary artery blood flow velocity and vasodilator reserve in man. *Circulation* 1985;72:82-92.
13. Rossen JD, Simonetti I, Marcus ML, Winniford MD. Coronary dilation with standard dose dipyridamole and dipyridamole combined with hand-grip. *Circulation* 1989;79:566-572.
14. Walsh MN, Geltman EM, Steele RL, et al. Augmented myocardial perfusion reserve after coronary angioplasty quantified by positron emission tomography with H₂¹⁵O. *J Am Coll Cardiol* 1990;15:119-127.
15. Bergmann SR, Herrero P, Markham J, Weinheimer CJ, Walsh MN. Noninvasive quantification of myocardial blood flow in human subjects with oxygen-15-labeled water and positron emission tomography. *J Am Coll Cardiol* 1989;14:639-642.
16. Vanoverschelde JL, Wijns W, Bol A, et al. Direct comparison between N-13 ammonia and O-15 water for quantitating myocardial blood flow [Abstract]. *Circulation* 1990;82:III-477.
17. Choi Y, Hawkins RA, Huang SC, et al. Parametric images of myocardial metabolic rate of glucose generated from dynamic cardiac PET and 2-[¹⁸F]fluoro-2-deoxy-D-glucose studies. *J Nucl Med* 1991;32:733-738.
18. Lockwood AH, McDonald JM, Reiman RE, et al. The dynamics of ammonia metabolism in man. *J Clin Invest* 1979;63:449-460.
19. Rosenspire KC, Schwaiger M, Mangner TJ, Hutchins GD, Sutorik A, Kuhle DE. Metabolic fate of [¹³N]ammonia in human and canine blood. *J Nucl Med* 1990;31:163-167.
20. Heymann M, Payne B, Hoffman J, Rudolph A. Blood flow measurements with radionuclide-labeled particles. *Prog Cardiovasc Dis* 1977;20:55-79.
21. Kuhle W, Porenta G, Huang SC, Phelps ME, Schelbert HR. Issues in the quantitation of reoriented cardiac PET images. *J Nucl Med* 1992;33:1235-1242.
22. Porenta G, Kuhle W, Czernin J, et al. Gated PET FDG imaging permits parameter estimation of cardiac geometry: validation using gated MR imaging and echocardiography [Abstract]. *J Nucl Med* 1991;32:927.
23. Gambhir SS. Quantification of the physical factors affecting the tracer kinetic modeling of cardiac positron emission tomography data. PhD dissertation. University of California, Los Angeles, 1990.
24. Weinberg IN, Huang SC, Hoffman EJ, et al. Validation of PET-acquired input functions for cardiac studies. *J Nucl Med* 1988;29:241-247.
25. Gambhir SS, Schwaiger M, Huang SC, et al. Simple noninvasive quantification method for measuring myocardial glucose utilization in humans employing positron emission tomography and fluorine-18-deoxyglucose. *J Nucl Med* 1989;30:356-366.
26. Krivokapich J, Huang SC, Phelps ME, MacDonald NS, Shine KI. Dependence of N-13 ammonia myocardial extraction and clearance on flow and metabolism. *Am J Physiol* 1982;242:H536-H542.
27. Patlak CS, Blasberg RG, Fenstermacher JD. Graphical evaluation of blood-to-brain transfer constants from multiple-time uptake data. *J Cereb Blood Flow Metab* 1983;3:1-7.
28. Patlak CS, Blasberg RG. Graphical evaluation of blood-to-brain transfer constants from multiple-time uptake data. Generalizations. *J Cereb Blood Flow Metab* 1985;5:584-590.
29. Chen BC, Huang SC, Germano G, et al. Noninvasive quantification of hepatic arterial blood flow with nitrogen-13-ammonia and dynamic positron emission tomography. *J Nucl Med* 1991;32:2219-2208.
30. Nitzsche EU, Choi Y, Killion D, et al. Simplified quantification of regional cortical renal blood flow [Abstract]. *Radiology* 1992;185(p):139.